Effect of Weissenberg number on polymer-laden turbulence

Sajjad ur Rehman
School of Humanities and Sciences, College of Aeronautical Engineering (CAE),
National University of Sciences and Technology, Risalpur, Pakistan

Junghoon Lee
School of Mathematics and Computing, Yonsei University, 03722 Seoul, Korea

Changhoon Lee[*]
School of Mathematics and Computing, Yonsei University, 03722 Seoul, Korea
and Department of Mechanical Engineering, Yonsei University, 03722 Seoul, Korea

Direct numerical simulation of polymer-laden turbulent flow is performed for the investigation of the two-way interaction. Lagrangian dynamic simulation is adopted for a finitely extensible nonlinear elastic (FENE-2) dumbbell model to observe polymer dynamics in turbulent flow. The impact of the polymers on fluid momentum is described using the elastic force between two beads. The elasticity of the polymer is characterized using the Weissenberg number, $\mathrm{We}^* = \frac{\tau_p}{\tau_k}$, where τ_p and τ_k denote the elasticity timescale and the Kolmogorov timescale, respectively. We observe that for $\mathrm{We}^* \leqslant 1.0$ most of the polymers are in a coiled state and the hydrodynamic properties of fluid remain unchanged. The coil-stretch transition is observed at approximately $\mathrm{We}^* = 3.0$. The highly stretched polymers in turn contribute to significant turbulence modification for large values of the Weissenberg number. The effect of the Weissenberg number on various turbulent statistics is computed and analyzed. The highly stretched polymers tend to rotate around the vortical structures. The feedback force effectively suppresses the turbulence structures for large values of the elasticity parameter. The effect of We^* on the alignment between the end-to-end distance vector, vorticity vector, and the eigenvector of the rate of strain tensor is presented. A better insight into the effect of polymers on turbulence is obtained through the direct force modeling in stationary turbulence although the effect itself has been known for a long time.

I. INTRODUCTION

It has been known that polymer additives are responsible for turbulent drag reduction [1]. Owing to their various applications to industrial devices, such as irrigation pumps, water circulating devices including heating-cooling systems, fire-fighting equipment, and long-distance pipelines for liquid transportation [2], numerous investigations have been carried out to understand how polymers interact with turbulence for several decades.

Traditionally, most numerical studies have used a continuum or often referred to as the Eulerian-Eulerian approach to investigate the dynamics of the dilute polymer solution. In this approach, constitutive equations for polymer models [3] such as Oldroyd-B or finitely extensible nonlinear elastic - Peterlin (FENE-P) models are described in an Eulerian frame. The drag reduction associated

---

*Corresponding author: clee@yonsei.ac.kr

with polymers was explained by using these models. However, the Oldroyd-B model, which is equivalent to the Hookean model, is unphysical while the FENE-P model requires closure approximation. In the FENE-P model, the polymer chain is represented by the dumbbell model in which two beads are connected by a finitely extensible elastic spring. The conformation tensor was used to characterize the averaged second moment of the polymer chain end-to-end distance vector. Then the polymer stress tensor was constructed to describe the effect of polymers on the turbulent flow. The fully coupled direct numerical simulation (DNS) has been carried out to observe drag reduction due to polymers for different flow geometries [3–9]. The statistically steady homogeneous isotropic turbulence laden with polymers was investigated using the FENE-P model [10–12]. They reported a significant reduction in kinetic energy, dissipation, and modification in kinetic energy spectrum. This approach, however, has some drawbacks from the analysis point of view. Detailed behavior of polymers such as orientation and stretching or the resulting interaction between polymers and turbulence, which can provide better insight into dynamics, cannot be easily examined.

The Eulerian-Lagrangian approach, in which DNS is performed for Naiver-Stokes equations and a significant number of polymers are tracked in the Lagrangian framework, became feasible due to advancement of computing resources. This approach has been used to study the behavior of passive polymers (i.e., those having no effect on fluid) [13–15] and then extended to where the effect of polymers on the flow field is considered [16–19]. This approach is useful to get detailed information on the behavior of polymers such as the polymer orientation and extensibility for different values of the Weissenberg number. However, the use of interpolation and a large number of polymers for statistical convergence result in a huge computational cost, which is a drawback of this approach.

Within the one-way coupling range, the Lagrangian nature of polymers has been studied in DNS of stationary homogeneous isotropic turbulence by Jin and Collins [13]. They considered finitely extensible nonlinear elastic spring models for polymers with N number of beads, the so-called FENE-N model, where $N = 2, 5, 10$, and 20, and compared their performance with the FENE-P model. For large Weissenberg numbers, they found the error in magnitude of the polymer stress to be around 10–15% between the FENE-N and FENE-P models. Another aspect they described in the FENE-P model is the spatial resolution requirements. Due to the hyperbolic nature of the conformation tensor, discontinuities were observed in the polymer stress tensor magnitude and orientation. Watanabe and Gotoh [14] analyzed polymer statistics for the FENE-20 model and showed that polymer elongation is highly dependent on the value of the Weissenberg number in their one-way coupled Lagrangian simulation of polymers. They found that the coil-stretch transition occurred at We = 3–4. They also found that the FENE-2 (dumbbell) model can reproduce similar statistics for polymers if a mapping formula for comparison between the two models, proposed by Jin and Collins [13], is properly used. Vincenzi *et al.* [15] compared the FENE-P and FENE-2 models in their one-way coupled simulation of forced homogeneous isotropic turbulence. In their DNS study, only a qualitative agreement was observed between the results of these two models. A weak tendency was observed for the alignment of polymers with both the eigenvectors of the strain rate tensor and vorticity vector of the fluid. For large Weissenberg numbers, the FENE-P model overpredicted the probability density functions (PDFs) of large extensions of polymers and underpredicted the correlation times of the polymer extension and orientation.

There have been several attempts to consider the two-way coupling interaction between polymers and turbulence in the Lagrangian simulation. For example, Peters and Schumacher [16] used the point force method, which is popularly used in the two-way coupled DNS with the Lagrangian point-particle tracking technique [20–26], to investigate the two-way effect of polymers in homogeneous shear turbulence in their DNS study for $1 \leqslant \text{We} \leqslant 25$. As the Weissenberg number increased, the FENE dumbbells were aligned in the mean flow direction. When vortex stretching or biaxial strain dominated the flow, the dumbbells were highly stretched. Watanabe and Gotoh [17,18], ,19] investigated the effect of polymers on turbulence in their DNS of decaying isotropic turbulence for a wide range of Weissenberg numbers. In their studies, the two-way coupling effect in the Navier-Stokes equations was modeled by the divergence of the polymer stress tensor. A large number of polymers was used to observe significant turbulence modification in their studies. For

$1 \leqslant \mathrm{We} \leqslant 25$, a reduction in fluid dissipation, kinetic energy, and its spectrum was observed and the polymer feedback forces played a vital role in suppressing vortical structures as the Weissenberg number increased. For $25 \leqslant \mathrm{We} \leqslant 200$, power-law spectra for kinetic energy and pressure variance were obtained when the ensemble-averaged potential energy for polymers was much greater than the average fluid kinetic energy.

Those studies on two-way coupling in the Lagrangian simulations mentioned above are investigations on polymer dynamics in decaying turbulence or homogeneous shear turbulence. The coupling between the polymer and turbulence in decaying turbulence was implemented using a polymer stress tensor, which requires a large number of polymers such as $O(10^{13})$ to obtain the convergent solution, resulting in huge computational cost. To the best of our knowledge, the effect of two-way coupling was not fully investigated for a wide range of Weissenberg numbers in stationary homogeneous isotropic turbulence. In this study of two-way coupled DNS of stationary homogeneous isotropic turbulence, we use the point-force formulation for the interaction between polymers and turbulence in the FENE-2 model since the FENE-2 model captures most dynamics of the FENE-N model with higher N [14]. The direct comparison between the one-way and two-way coupling results helps us understand the behavior of polymers in stationary turbulence. The coil-stretch transition in polymers in the presence of coupling is investigated. The alignment of highly stretched polymer end-to-end distance vector with the principal axis of the rate of strain tensor is also investigated. Another aspect, which we focus on, is the polymer effect on vorticity and enstrophy dynamics. The spectral analysis and the polymer's influence on kinetic energy spectra, dissipation, and energy transfer rate are also investigated for a wide range of Weissenberg numbers.

This paper is organized as follows. Section II on the computational approach describes the governing equation for fluid motion, polymer model equations, two-way coupling force, numerical simulation, and the parameters used in current problem. Section III provides various results for the interaction between turbulence and polymers. Finally, the conclusion is given in Sec. IV.

II. COMPUTATIONAL APPROACH

A. Governing equations

The governing equations for fluid motion in polymer-laden incompressible turbulent flow is the continuity equation and the Navier-Stokes equation given by

$$\nabla \cdot \boldsymbol{u} = 0, \tag{1}$$

$$\frac{\partial \boldsymbol{u}}{\partial t} + (\boldsymbol{u} \cdot \nabla)\boldsymbol{u} = -\frac{1}{\rho_f}\nabla p + \nu_f \nabla^2 \boldsymbol{u} + \boldsymbol{f}_e + \boldsymbol{f}, \tag{2}$$

where $\boldsymbol{u}$, ν_f, and ρ_f denote velocity vector, the kinematic viscosity, and density of fluid, respectively. $\boldsymbol{f}_e$ is an external forcing to maintain stationary turbulence. $\boldsymbol{f}$ represents the coupling between polymers and turbulence. Detailed descriptions of the external and coupling forces are provided in Secs. II C and II B, respectively.

Among various polymer models [3], the dumbbell model is adopted. A couple of mass-less beads connected by nonlinear spring is referred to as a finitely extensible nonlinear elastic (FENE-2) model. Polymers can translate, rotate, and stretch when advecting through fluid. The dilute polymer solution is considered in the Lagrangian frame and the interaction between different dumbbells is neglected. The trajectory of the mth dumbbell ($m = 1, 2, ..., N_r$) (N_r: real number of dumbbells) can be described by a set of equations for end-to-end distance vector $\boldsymbol{Q}^{(m)}$ and the center of mass $\boldsymbol{Q}_c^{(m)}$ position vector. The polymer model equations for the mth polymer are written as [19]

$$\frac{d\boldsymbol{Q}^{(m)}}{dt} = \boldsymbol{u}_1^{(m)} - \boldsymbol{u}_2^{(m)} - \frac{\gamma(z)}{2\tau_p}\boldsymbol{Q}^{(m)} + \frac{Q_0}{\sqrt{2\tau_p}}\left(\boldsymbol{\xi}_1^{(m)} - \boldsymbol{\xi}_2^{(m)}\right), \tag{3}$$

$$\frac{d\boldsymbol{Q}_c^{(m)}}{dt} = \frac{1}{2}\left(\boldsymbol{u}_1^{(m)} + \boldsymbol{u}_2^{(m)}\right) + \frac{Q_0}{\sqrt{8\tau_p}}\left(\boldsymbol{\xi}_1^{(m)} + \boldsymbol{\xi}_2^{(m)}\right), \tag{4}$$

where $\boldsymbol{Q}^{(m)}(t) = \boldsymbol{q}_1^{(m)} - \boldsymbol{q}_2^{(m)}$ and $\boldsymbol{Q}_c^{(m)}(t) = (\boldsymbol{q}_1^{(m)} + \boldsymbol{q}_2^{(m)})/2$ with $\boldsymbol{q}_1^{(m)}$ and $\boldsymbol{q}_2^{(m)}$ denoting the bead positions. $\boldsymbol{u}_{1,2}^{(m)}$ is the fluid velocity at a bead position. The $\gamma(z) = 1/(1 - z^2)$ represents finitely extensible nonlinear elastic model [3] with $z = |\boldsymbol{Q}^{(m)}(t)|/Q_{\max}$. The Brownian force in base is represented by $\boldsymbol{\xi}_{1,2}^{(m)}(t)$; it is also referred to as random force. The random force obeys Gaussian statistics with white-in-time correlation [19]:

$$\left\langle \xi_{\alpha,i}^{(m)}(t) \right\rangle = 0, \tag{5}$$

$$\left\langle \xi_{\alpha,i}^{(m)}(t) \xi_{\beta,j}^{(n)}(s) \right\rangle = \delta_{\alpha\beta} \delta_{nm} \delta_{ij} \delta(t - s), \tag{6}$$

where $\alpha, \beta = 1, 2$, $i, j = 1, 2, 3$, and $n, m = 1, 2, ..., N_r$. The angle bracket $\langle ... \rangle$ here denotes the ensemble average over the computational number of dumbbells. The polymer relaxation time is $\tau_p (\equiv \zeta/4H)$, where $\zeta = 6\pi \nu_f \rho_f r_b$, the friction coefficient, H is the spring constant, and r_b is the bead radius. $Q_0(\equiv \sqrt{k_B T/H})$ is the equilibrium length of the polymers when $\boldsymbol{u}(\boldsymbol{x}, t) = 0$. k_B and T represent the Boltzmann constant and absolute temperature, respectively. The elastic force between two beads prevents the polymers from stretching beyond their maximum stretching length $Q_{\max}$.

B. Coupling between polymers and turbulence

A conventional numerical approach to investigate the interaction between polymers and turbulence is the continuum approach, in which the dynamics of fluid and polymers is simulated in the Eulerian frame [4,5,27]. The continuum approach has been applied to various polymers such as Oldroyd-B, FENE-P, Maxwell, and Giesekus models [3,6,8,28]. Recently, the Brownian dynamic simulation in the Lagrangian frame was introduced as an alternative to the continuum approach to study the polymer dynamics. In this approach, various models such as bead-rod chain, bead spring chain (FENE-N), and bead spring dumbbell (FENE-2) were tested. These models require high computational cost, but they are supposed to simulate dynamics more accurately [13,14,16,18,19,29].

Particularly, the coupled hybrid Eulerian-Lagrangian simulation using a dumbbell model for various values of elasticity parameter was applied to polymer-laden decaying turbulence [19]. The coupling between polymers and turbulence was described by introducing polymer stress tensor [18,19]. However, to achieve statistically convergent results and proper turbulence modification, a huge number of dumbbells was necessary. Two-way coupling simulation in shear turbulence for FENE dumbbell model (bead inertia $\neq 0$) was performed by Peters and Schumacher [16]. The polymer-turbulence coupling was modeled by direct implementation of forces acting between each bead and turbulence. In the present study, we adopt the direct force approach of Peters and Schumacher [16]. We also tested the polymer stress approach used in Refs. [14,19], but we found that the polymer stress approach requires computing spatial derivatives of delta functions, which introduces much noise, and for this reason a huge number of polymers is necessary to guarantee converged statistics. Meanwhile, the direct approach to computing coupling forces requires the implementation of δ-function forces only, and thus converged calculation requires a much fewer number of polymers than the polymer stress approach.

In the absence of polymer inertia, the elastic force between beads of the mth dumbbell is balanced by drag force due to the stretching motion of fluid and Brownian force. The back-reaction force by the first bead of a polymer is

$$\boldsymbol{F}_1^{(m)} = -H\gamma(z)\big(\boldsymbol{q}_1^{(m)} - q_2^{(m)}\big), \tag{7}$$

while on the second bead, $\boldsymbol{F}_2^{(m)} = -\boldsymbol{F}_1^{(m)}$. Then, the back-reaction force by all polymers at the Eulerian grid points is

$$\boldsymbol{f}(\boldsymbol{x}, t) = \frac{1}{\rho_f} \sum_{m=1}^{N_c} \big[\delta\big(\boldsymbol{x} - \boldsymbol{q}_1^{(m)}\big)\boldsymbol{F}_1^{(m)} + \delta\big(\boldsymbol{x} - \boldsymbol{q}_2^{(m)}\big)\boldsymbol{F}_2^{(m)}\big]. \tag{8}$$

TABLE I. Forcing parameters.

N	ν_f	κ_f	σ_f	T_L^f
96^3	0.03	$2\sqrt{2}$	0.055	0.4312

This force is projected on the nearest eight grid points of computational mesh using linear interpolation weights, which is expressed for two bead positions $\forall j = 1, 2$;

$$W\left(\boldsymbol{x} - \boldsymbol{q}_j^{(m)}\right) = \begin{cases} \frac{1-r_i}{\Delta V} & \text{if} \quad \left|\boldsymbol{x} - \boldsymbol{q}_j^{(m)}\right| < \Delta x_i, \\ 0 & \text{otherwise} \end{cases}$$

where $i = 1, 2, 3$, $r_i = |\boldsymbol{x} - q_j^{(m)}|/\Delta x_i$ is the distance between the bead and computational node. ΔV is the volume of a computational cell with grid size Δx_i.

C. Numerical simulation

A pseudospectral method is used for the numerical simulation of Navier-Stokes equations [Eq. (II C)]. The primitive variables in the governing equations are expanded using discrete Fourier series with periodic boundary conditions in three spatial directions. The computational domain is a cubic box of size $L_{\text{box}}^3 = (2\pi)^3$ with 96^3 number of grids. Turbulence is maintained artificially by a statistically stationary force at low wave number modes $0 < \kappa \leqslant \kappa_f$, where κ is the magnitude of a wave number vector $\boldsymbol{\kappa}$ [30]. The external force $\boldsymbol{f}_e$ in Eq. (II C) is formulated in the Fourier space,

$$\hat{\boldsymbol{f}}_e = \hat{\boldsymbol{F}}_e - \frac{\boldsymbol{\kappa}}{\kappa^2}(\boldsymbol{\kappa} \cdot \hat{\boldsymbol{F}}_e), \tag{9}$$

where $\hat{\boldsymbol{f}}_e$ is the Fourier coefficient of $\boldsymbol{f}_e$ and $\hat{\boldsymbol{F}}_e$ is a stochastic process characterized by a timescale T_L^f and the standard deviation σ_f satisfying the Langevin equation,

$$d\hat{\boldsymbol{F}}_e = -\frac{\hat{\boldsymbol{F}}_e}{T_L^f}dt + \sqrt{\frac{2\sigma_f^2}{T_L^f}}d\boldsymbol{W}_t, \tag{10}$$

where $d\boldsymbol{W}_t$ is an increment of the Wiener process obeying the Gaussian distribution with mean zero and variance dt. The values for T_L^f and σ_f are chosen such that the timescale is larger than the eddy turnover time, and the forcing parameters are listed in Table I. Although Eswaran and Pope [21,30] provided the estimate for predicted values of parameters such as dissipation rate and the Kolmogorov length scale, these forcing parameters are tuned to generate turbulence at a specific Reynolds number for the given grid number.

Although the polymer dynamics was investigated in decaying turbulence [18,19], the role of polymers in modifying stationary isotropic turbulence has not been discussed for a wide range of Weissenberg numbers yet. Furthermore, by considering stationary turbulence, we can make more quantitative analysis from the time-averaged statistics that are free from transient behavior due to the initial condition. As shown in Fig. 2(a), this artificial effect due to the initial condition of polymers lasts for a long time and time-averaged statistics are obtained over a time span of $t = 25T_e$, where T_e is an eddy turn-over time. The same initial condition was also used in decaying isotropic turbulence in Refs. [18,19].

The polymer model Eqs. (3) and (4) are solved in the Lagrangian frame. The polymers are randomly distributed initially [18,19] in the flow domain. The initial configuration is $Q^{(m)}(0) = \sqrt{3}Q_0\hat{\boldsymbol{n}}^{(m)}$, where $\boldsymbol{n}^{(m)}$ is a random unit vector.

TABLE II. Artificial factor N_r/N_c and the computational number of polymers N_c used in test for We* $= 5.0$.

Case	A	B	C	D	E
N_r/N_c (in 10^6)	0.625	1.25	2.5	5.0	10
N_c (in 10^6)	21.088	10.544	5.272	2.636	1.318

The third-order, three-stage Runge-Kutta method is used for time advancement of both fluid and polymer phases. For the interpolation of fluid velocity at the bead position, a four-point Hermite interpolation is used. A complete description of the interpolation scheme is provided by Choi *et al.* [31].

The length and timescale parameters of polymers are the equilibrium length Q_0, the maximum stretching length Q_{max}, and the relaxation time τ_p. The values of these parameters are determined from the experimental study performed by Ouellette *et al.* [32] and the numerical simulation performed by Watanabe and Gotoh [18] in decaying turbulence. The initial value of the Kolmogorov length scale $\eta_k(0)$ is used to set the dumbbell equilibrium $Q_0 = 0.03\eta_k(0)$, maximum stretching $Q_{max} = 0.3\eta_k(0)$, and bead radius $r_b = 7 \times 10^{-5}\eta_k(0)$ [18]. The nondimensional Weissenberg number We* $= \tau_p/\tau_k(0)$ is used as the key parameter in this study for different values of polymer relaxation times with a fixed value of $\tau_k(0)$, which is the Kolmogorov timescale of unladen turbulence. Alternatively, the Weissenberg number (hereinafter referred to as We), We $= \tau_p/\overline{\tau_k}$ based on time-averaged value $\overline{\tau_k}$ is used.

The volume fraction ϕ_v is defined as $\phi_v = (8\pi N_r/3)(r_b/L_{box})^3$, where N_r represents the real number of dumbbells and L_{box} is the length of the domain. The value of volume fraction $\phi_v = 2.525 \times 10^{-6}$ is found to be sufficient in the current study to observe the significant turbulence modification with reasonable computational cost. The computational number of dumbbells N_c was fixed using the artificial factor N_r/N_c as suggested in previous studies [18,19,33] both in particle- and polymer-laden turbulence.

To fix the value of N_r/N_c, a test with five different values was performed for We* $= 5.0$ as shown in Table II. If the number of computational dumbbells is very small and large N_r/N_c is used, it cannot represent real physics properly. However, if a very large number of dumbbells are tracked, computational cost rises. To find the optimum value for the artificial factor, the turbulence and polymer statistics for different values of the artificial factor under the same physical condition were obtained and compared. All the statistics for these tests are computed for We* $= 5.0$ since coil-stretch transition (presented below) in polymers is observed at We* $= 3.0$ and thus most polymers are stretched enough at We* $= 5.0$, significantly modifying turbulence.

The polymer behavior is captured by the magnitude of end-to-end distance vector $|\boldsymbol{Q}(t)|$ [18], which is used to represent the elongation of polymers. The time-averaged magnitude of the end-to-end distance vector is denoted by $Q = \overline{|\boldsymbol{Q}|}$. For We* $= 5.0$, the time-averaged Q value normalized with the maximum stretching length for different values of N_r/N_c is shown in Fig. 1(a). The variation in polymer elongation is not significant as N_r/N_c decreases. The PDF of magnitude is shown in Fig. 1(b), indicating that the distribution converges as N_r/N_c decreases.

The time-averaged Eulerian quantities of modified turbulence such as dissipation rate ε, kinetic energy q, and the mean vorticity magnitude $\omega' = \sqrt{\overline{\omega^2}}$ for different values of N_r/N_c are shown in Fig. 1(c). The mean values are normalized by the corresponding values for polymer-free case values. As N_r/N_c decreases, all statistics tend to converge to values smaller than 1, indicating that there is a reduction in mean dissipation, kinetic energy, and rms of vorticity. This convergent behavior of statistics justifies the use of point force approximation for the polymers feedback force. Based on this test, we decided to use $N_c = 1.0544 \times 10^7$ and the corresponding $N_r/N_c = 1.25 \times 10^6$. The computational number of dumbbells used in the present study is less than $N_c = 5.04 \times 10^8$ used in previous studies [17–19].
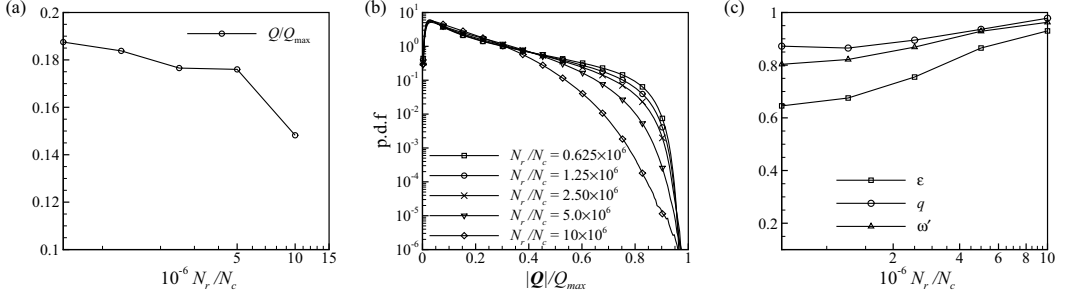
FIG. 1. Numerical test with different N_r/N_c: (a) time-averaged magnitude of the end-to-end distance vector; (b) PDF of magnitude of end-to-end distance vector; and (c) time-averaged mean dissipation, kinetic energy, and rms of vorticity.

III. RESULTS

In the following sections, the simulation results for polymer-laden turbulent flow are presented. The simulations were performed with $N_c = 1.0544 \times 10^7$ based on the test given earlier. The ensemble average for polymer quantities is performed over the computational number of dumbbells, while the spatial average of turbulence quantities is carried out in the Eulerian frame. The ensemble/spatial average is denoted by angle brackets $\langle \cdot \rangle$, while time- and space/ensemble-averaged quantities are represented by an overline.

The simulations are performed for a wide range of Weissenberg numbers listed in Table III with corresponding values of polymer relaxation time. The time variation of statistics is plotted using the nondimensional time $t^* = t/\tau_k(0)$. When $t^* \geqslant 275$, the statistically steady state is observed for turbulent flow and time-averaged statistics are obtained in the range $275 \leqslant t^* \leqslant 460$.

A. Polymer statistics

In this section, the behavior of polymers is first described in terms of statistics. The dumbbells advecting through fluid are influenced by three kinds of forces: drag by fluid motion, elastic force

TABLE III. Cases considered in the present study for polymer-laden turbulence. $\varepsilon_0(= 10.58)$ and $q_0(= 10.303)$ are values for unladen turbulence. $\text{We}^* = \tau_p/\tau_{k,0}$ and $\text{We} = \tau_p/\tau_k$ where $\tau_{k,0}$ is the Kolmogorov timescale for unladen turbulence.

| Re_λ	τ_p	We^*	We	$\varepsilon/\varepsilon_0$	q/q_0	τ_k	η_k	l_e	T_e	λ	$\kappa_{\max}\eta_k$
47.21				1.0	1.0	0.054	0.040	0.653	1.712	0.419	1.80
45.31	0.0054	0.1	0.10	0.98	0.96	0.054	0.040	0.632	1.611	0.533	1.80
45.66	0.027	0.5	0.503	0.97	0.95	0.054	0.040	0.637	1.629	0.535	1.80
46.58	0.054	1.0	1.03	0.94	0.97	0.053	0.040	0.631	1.656	0.532	1.80
43.86	0.108	2.0	2.06	0.93	0.90	0.053	0.040	0.601	1.517	0.534	1.80
47.15	0.163	3.0	2.97	0.86	0.93	0.055	0.041	0.670	1.725	0.538	1.84
48.30	0.190	3.5	3.49	0.87	0.96	0.056	0.040	0.679	1.781	0.561	1.83
48.71	0.218	4.0	3.85	0.81	0.94	0.057	0.041	0.711	1.836	0.569	1.86
49.48	0.272	5.0	4.64	0.75	0.92	0.059	0.042	0.750	1.917	0.584	1.90
52.60	0.544	10	8.08	0.57	0.85	0.067	0.045	0.913	2.249	0.612	2.03
52.51	1.088	20	14.80	0.47	0.77	0.074	0.047	0.998	2.347	0.678	2.13
53.40	2.176	40	28.75	0.45	0.76	0.076	0.047	1.042	2.439	0.684	2.14
55.31	4.352	80	55.84	0.42	0.77	0.080	0.048	1.112	2.609	0.690	2.19
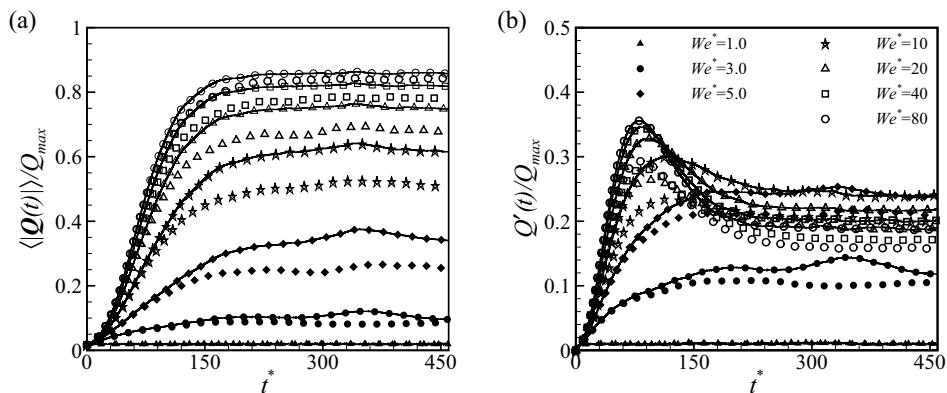
FIG. 2. Polymer statistics of the end-to-end distance magnitude (a) mean and (b) rms; here the solid line with symbol represents the one-way coupling case results.

between two beads, and thermal fluctuations due to Brownian motion. The role of the elasticity parameter in the alteration of polymer configuration (i.e., from coiled to maximum stretched state) is inevitable [14,18]. The Eulerian and Lagrangian statistics were obtained for a wide range of elasticity parameter We^*. The rms of the end-to-end distance-vector magnitude is represented by $Q'(t) = \sqrt{\langle [|\boldsymbol{Q}(t)| - Q(t)]^2 \rangle}$. The ensemble averaged values of the mean and rms quantities were normalized with the maximum stretching length. The time variation of the average magnitude of the end-to-end distance vector in the early transient period is presented in Fig. 2(a). The comparison between the one- and two-way coupling simulations is shown only for selected values of the elasticity parameter for the sake of clarity. We find that the averaged values remain very small in both cases, when $We^* \leqslant 2.0$, although for reference only cases with $We^* = 1.0$ are shown in Fig. 2(a). This indicates that most polymers are in a coiled configuration, where the elastic force between two beads dominates over the stretching motion due to fluid. There is no significant contribution from polymer feedback force in the two-way coupling case for these two values. The increment in mean value is observed for $We^* \geqslant 3.0$ as shown in Fig. 2(a) for both cases. This observation is consistent with previously reported studies [18]. The polymers are more stretched in case of one-way coupling compared to two-way coupling. The stretching in the polymers in two-way coupling cases is limited due to the presence of feedback force. The stretched polymers contribute much to the feedback force and the resulting suppression in turbulence is observed, as will be discussed later.

The comparison between the rms $Q'(t)$ for different values of We^* in both one- and two-way coupling cases is shown in Fig. 2(b). The rms for $We^* \leqslant 2.0$ is very small, similar to the mean value. The fluctuations increase for $We^* \geqslant 3.0$. However, when $We^* \geqslant 10.0$, the fluctuations rapidly increase and the peak value is observed at approximately $t^* = 91$ and then the decay is observed. This decay is more pronounced for $We^* = 20, 40, 80$. This kind of different transient behavior of polymers for different We^* is due to different stiffness of the polymers; Stiff polymers with small We^* show overdamped behavior, while less stiff polymers with large We^* tend to be underdamped. A large value of the converged rms for $We^* = 10$ is observed, as compared to other values when $t^* \geqslant 183$. Most polymers are stretched toward maximum stretching length, while there exist some polymers in a coiled configuration. This contributes much to the fluctuations, resulting in an increase in the rms value. For $We^* \geqslant 20$, the polymers are highly stretched and the peak is completely shifted toward the maximum stretching length [see Fig. 4(b)]. Both the mean stretching and its rms statistics indicate that a statistically steady state is attained when $t^* \geqslant 275$.

The coil-stretch transition [34,35] (hereinafter referred to as CST) is observed in a polymer solution when the value of the elasticity parameter reaches its threshold value. When it occurs, the stretching dominates over the polymer molecule relaxation, or in other words, the characteristic
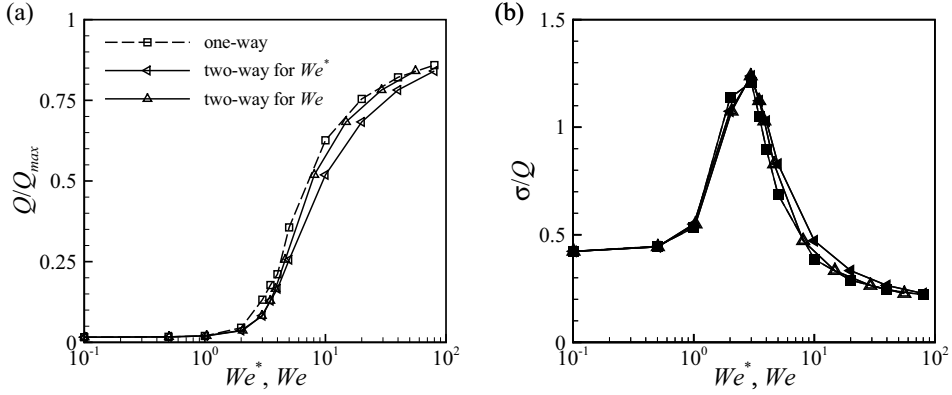
FIG. 3. Effect of We*, We on variations in (a) Q and (b) σ for both one-way and two-way coupling cases.

timescale of turbulence (τ_k) is smaller than the polymer relaxation time (τ_p). The CST was previously discussed in stationary turbulence for passive polymers by Watanabe and Gotoh [14]. For dumbbell and polymer chain (FENE-20) models, CST was observed when elasticity parameter is in the range of We* = 3–4. In the present study, we used wide range of elasticity parameter $0.1 \leqslant \text{We}^* \leqslant 80$ to compute the CST in the presence of two-way coupling for stationary turbulence. For this purpose, the mean value of the end-to-end distance-vector magnitude and mean standard deviation (referred to as σ) $\sigma = (\overline{|\boldsymbol{Q}|^2 - Q^2})^{1/2}$ are calculated for different values of elasticity parameter.

Figure 3(a) presents the comparison between the time-averaged values Q of both one- and two-way coupling simulations. The averaged value is the same for both cases when We*, We $\leqslant 1.0$. The polymers are more stretched in both cases as the elasticity parameter is increased. The averaged value for the one-way case is larger than the two-way coupling when plotted against We*. The two-way coupling effect on polymer statistics is enhanced, as elasticity parameter We* is increased. We observe that the stretching in polymers is constrained due to the presence of feedback force. However, this modification is compensated when the Weissenberg number is defined by τ_k of the modified turbulence.

As shown in Fig. 3(b), the mean standard deviation σ normalized by the mean value Q is obtained for both one- and two-way coupling cases. The value of σ is almost identical for both cases when
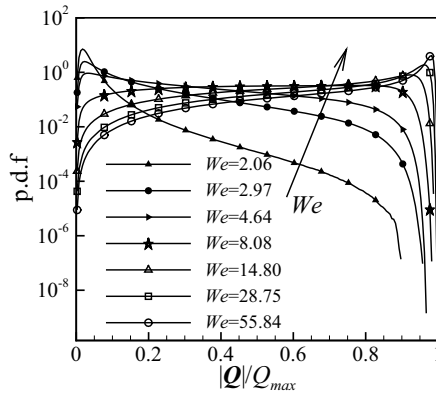

FIG. 4. Probability density function of the end-to-end distance vector magnitude for different values of the elasticity parameter.
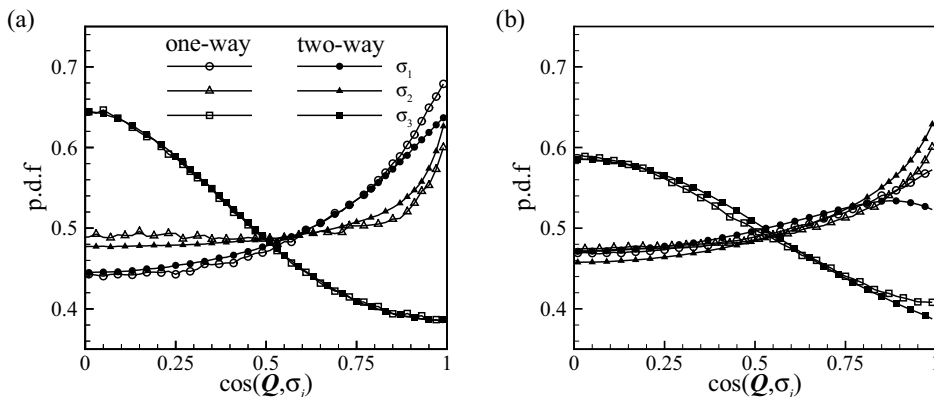
FIG. 5. Conditional PDF of cosine angle between end-to-end distance vector and eigenvectors of rate of strain tensor for (a) $We^* = 5.0$ and (b) $We^* = 20$. Owing to symmetry, only half of the PDF range is shown. Open symbols are for one-way coupling and closed symbols are for the two-way coupling case.

We^*, $We \leqslant 3.0$. When $We^* > 3.0$, however, the mean standard deviation is slightly larger for the two-way coupling case as compared to the one-way case. However, for $We > 3.0$, the curves are almost collapsed into each other. The peak value of the mean standard deviation of one- and two-way cases is observed when $We^* = 3.0$. The CST in this study is observed for $We^* = 3.0$ and $We = 2.97$. It seems that the CST in polymers is not affected by the presence of feedback forces at this volume fraction.

The CST can be investigated in the PDF of $|\boldsymbol{Q}|$ normalized with the maximum stretching length as shown in Fig. 4. The PDF for $We = 2.06$ clearly demonstrates that the peak is observed near zero and a few polymers are stretched towards the Q_{max}. When the value of We increased, the probability that polymers remains in coiled configuration was decreased. The polymers are gradually stretched due to increments in the elasticity parameter and the tail is extended toward maximum stretching length. For $We = 8.08$, the polymers are almost uniformly distributed except for both extreme values, where coiled and maximum stretched states are observed. The polymers are significantly stretched as We further increases, and the peak of the PDF emerges at the maximum stretching length. This finding is consistent with previously reported studies [18].

Next, we investigated the alignment between the polymer end-to-end distance vector and the principal axis of the rate of strain tensor at the polymer position since the motion of inertia-free polymer dumbbells is predominantly determined by the local straining motion of the fluid. Statistics of the cosine angles between these vectors, $\cos \theta_i = \boldsymbol{Q} \cdot \boldsymbol{\sigma}_i / |\boldsymbol{Q}||\boldsymbol{\sigma}_i|$, is investigated for the one- and two-way coupling cases, where $\boldsymbol{\sigma}_i$ is an eigenvector of eigenvalue λ_i of the rate of the strain tensor. The eigenvalues are ordered in such a way that $\lambda_1 > \lambda_2 > \lambda_3$, with the corresponding eigenvectors representing the most stretched, intermediate, and compressed directions, respectively. Figure 5 shows the conditional PDF of $\cos \theta_i$ for $i = 1, 2, 3$ for $We^* = 5.0$ and 20, when $|\mathbf{Q}(t)| > 0.65 Q_{max}$. $We^* = 5.0$ is chosen because the polymers are substantially stretched as the value is slightly larger than the value for which CST is observed. In the one-way coupling case, when $We^* = 5.0$, the peak value of the PDF for $\cos \theta_1$ and $\cos \theta_2$ is observed at 1. However, the peak value of the PDF of $\cos \theta_2$ is smaller than that of $\cos \theta_1$, which means that the end-to-end distance vector tended to preferentially align with the $\boldsymbol{\sigma}_1$ direction. For $\cos \theta_3$, the peak value of the PDF is observed at zero. When $We^* = 20$, however, we find that the most probable direction in this case is $\boldsymbol{\sigma}_2$ as presented in Fig. 5(b). This indicates that as the elasticity parameter is increased, the polymers are preferentially aligned with the $\boldsymbol{\sigma}_2$ direction in the one-way coupling case.

For the two-way coupling case, the peak value of the PDF of $\cos \theta_1$ and $\cos \theta_2$ is observed at 1 for $We^* = 5.0$. The polymers align with the $\boldsymbol{\sigma}_1$ or $\boldsymbol{\sigma}_2$ direction at equal probability as shown in
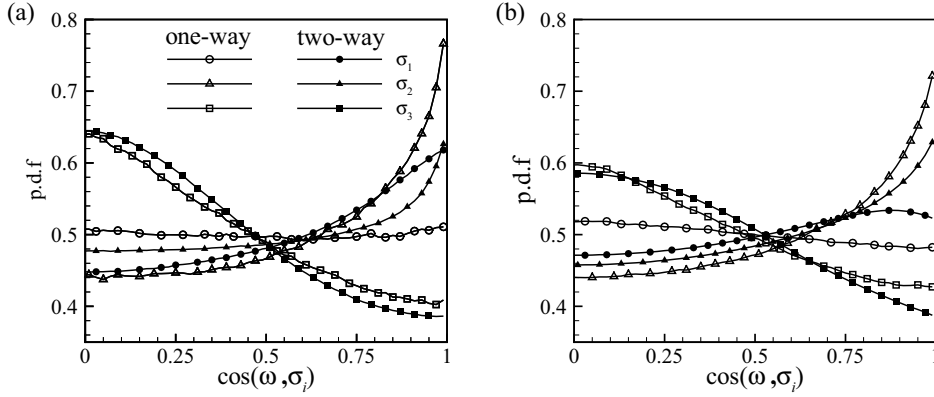
FIG. 6. Conditional PDF of cosine angle between the vorticity vector and eigenvectors of rate of strain tensor at polymer position for (a) $We^* = 5.0$ and (b) $We^* = 20$. Owing to symmetry, only half of the PDF range is shown. Open symbols are for one-way coupling and closed symbols are for two-way coupling case.

Fig. 5(a). This behavior is different from the one-way coupling case, where most of the polymers are preferentially aligned with the $\boldsymbol{\sigma}_1$ direction for the same value of We^*. This observation provides evidence that in the case of two-way coupling, the stretching in polymers is constrained due to feedback forces. Meanwhile, the peak value of the PDF is observed when $\cos\theta_3 = 0$. For $We^* = 20$, the most probable direction of the polymers is the direction of $\boldsymbol{\sigma}_2$, but a reduction in the peak value is noticeable as compared to the one-way case. However, in the case of two-way coupling with $We^* = 20$, the probability for $\boldsymbol{\sigma}_1$ is smaller compared with that of the one-way case. The shift in the peak location from 1 to 0.85 is observed for $\cos\theta_1$ in the two-way coupling case. This shift in the peak will be discussed in Sec. III B 2. We observe that for two-way coupling cases, the end-to-end distance vector tends to be preferentially aligned with the $\boldsymbol{\sigma}_2$ direction and this trend is insensitive to the Weissenberg number as long as $We^* > 10$. This alignment seems to be against intuition. However, since large We^* implies long response time of a polymer, the probability that an instantaneous alignment between the polymer and the local stretching motion would be decreased compared with polymers with low We^*. Furthermore, polymers tend to be strongly aligned with the local vorticity vector for large We^* as will be discussed in Sec. III B 2 and the vorticity vector has been known to align with $\boldsymbol{\sigma}_2$ [36].

Finally, we investigated the alignment between the vorticity vector and eigenvectors of strain rate tensor at the polymer position subject to the condition $|\mathbf{Q}(t)| > 0.65Q_{\max}$. The cosine angle between the two vectors, $\cos\theta_i = \boldsymbol{\omega} \cdot \boldsymbol{\sigma}_i / |\boldsymbol{\omega}||\boldsymbol{\sigma}_i|$, is evaluated for the one- and two-way coupling simulations for $We^* = 5.0$ and 20. For $We^* = 5.0$, the peak value of the PDF in $\cos\theta_1$ for one-way coupling case is observed at 1, while in two-way coupling case, the PDF value is smaller than that of the one-way case. The most probable direction that the vorticity vector aligned with is $\boldsymbol{\sigma}_2$ for the one-way coupling case, consistent with previous investigations in turbulent flow [36]. However, for the two-way coupling case, we found that the vorticity vector has equal probability to preferentially align with either $\boldsymbol{\sigma}_1$ or $\boldsymbol{\sigma}_2$ as shown in Fig. 6(a). This finding is similar to what we observed in the end-to-end distance vector in the two-way coupling case. For $\boldsymbol{\sigma}_3$, the probability is slightly higher compared to the one-way case when $\cos\theta_3 \leqslant 0.5$, and lower when $\cos\theta_3 > 0.5$. For $We^* = 20$, the vorticity vector in the two-way coupling case is aligned with the $\boldsymbol{\sigma}_2$. The peak value of the PDF for $\boldsymbol{\sigma}_1$ is shifted from $\cos\theta_2 = 1$ to 0.85 as shown in Fig. 6(b). A similar shift was observed in the end-to-end distance vector. This shift in peak location is due to the antialignment between the vorticity vector and vortex stretching vector, which will be discussed later.
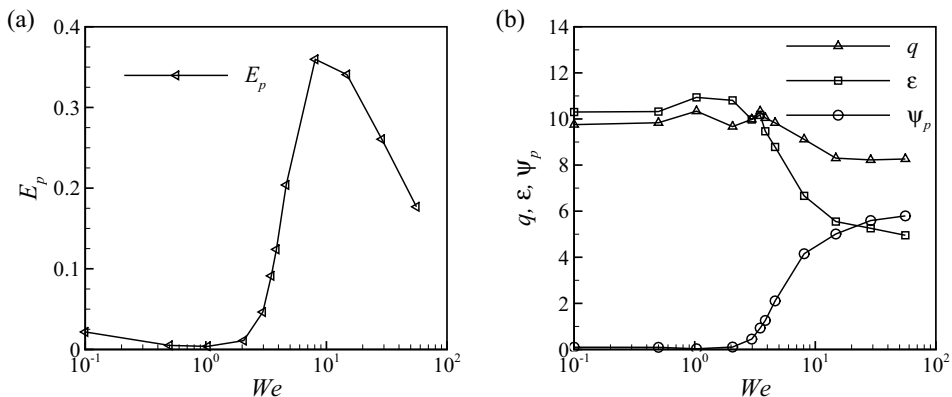
FIG. 7. Effect of the Weissenberg number on (a) E_p and (b) q, ε, and ψ_p.

B. Turbulence modification by polymers

The effect of the Weissenberg number on polymer statistics such as polymer elongation, coil-stretch transition, and alignment between the end-to-end distance vector and rate of strain tensor were presented in the previous section. In the following sections, the effect of the Weissenberg number on the turbulence modification by polymers is discussed.

1. Effect of Weissenberg number on turbulence

The physical parameters of the unladen turbulence, which is used for the initial condition and the reference case for comparison, are listed in Table III. The rms of the fluid velocity is given by $u' = \sqrt{\overline{u_i u_i}}$. The mean fluid dissipation and kinetic energy is defined as $\varepsilon_D = 2\nu_f \langle s_{ij} s_{ij} \rangle$ and $k = \frac{1}{2} \langle u_i u_i \rangle$, respectively, where $s_{ij} = \frac{1}{2}(\frac{\partial u_i}{\partial x_j} + \frac{\partial u_j}{\partial x_i})$ is the strain rate tensor. The time-averaged turbulence dissipation and kinetic energy are represented by $\varepsilon = \overline{\varepsilon_D}$ and $q = \bar{k}$, respectively.

The Taylor microscale is defined as $\lambda = \sqrt{15\nu_f u'^2/\varepsilon}$. The turbulent motion is characterized by Taylor microscale Reynolds number $\mathrm{Re}_\lambda = u'\lambda/\nu_f$. The Kolmogorov length and timescales are $\eta_k = (\nu_f/\varepsilon)^{1/2}$ and $\tau_k = (\nu_f^3/\varepsilon)^{1/4}$, respectively. The eddy length scale and turnover time are $l_e = u'^3/\varepsilon$ and $T_e = l_e/u'$, respectively.

Due to the elastic nature of polymers, the kinetic energy of turbulence transfers to elastic energy of polymers. The elastic energy of polymers $U_{\mathrm{pol}}(t)$ is defined as [19]

$$U_{\mathrm{pol}}(t) = -U_0 \frac{1}{N_c} \sum_{m=1}^{N_c} \ln \left[1 - \left(\frac{|\boldsymbol{Q}^{(m)}(t)|}{Q_{\max}} \right)^2 \right], \qquad (11)$$

where $U_0 = \frac{\nu_p}{2\tau_p}(\frac{Q_{\max}}{Q_0})^2$ is constant. $\nu_p = \nu_f \beta$ is polymer viscosity and β is the ratio of polymer to fluid viscosity known as zero-shear viscosity [19] and is given by $\beta = (3Q_0/4r_b)^2 \phi_v$. In the presence of polymers, the energy is transferred from kinetic to elastic or from elastic to kinetic energies. Therefore, there exists a trade-off between fluid kinetic energy and elastic energy of polymers [11,18,19]. The time-averaged value of the elastic energy of polymers is represented by $E_p = \overline{U_{\mathrm{pol}}}$ and is plotted against different values of We in Fig. 7(a). For We $\leqslant 1.03$, the averaged value of elastic energy is small, since most of the polymers are in a coiled configuration as shown in Fig. 3(a). However, when We > 2.06, an increment in averaged value was observed as compared to We $= 1.03$. This trend of increment in elastic energy value is enhanced as the We value is increased. The maximum value of averaged elastic energy is observed at We $= 8.08$. When We $\geqslant 14.80$, the depreciation in elastic energy value was observed, because the polymers are highly stretched, and

these stretched polymers suppress turbulence through the feedback force. As a result, the averaged kinetic energy is substantially decreased compared to its initial value as shown in Fig. 7(b). In this suppressed turbulence, the polymers are less stretched.

The evolution equation for mean-kinetic energy in the presence of feedback force f_i is derived from Naiver-Stokes equations, Eq. (II C),

$$\frac{dk}{dt} = \mathcal{F} - \varepsilon_D - \varepsilon_p, \tag{12}$$

where the first term on the right-hand side $\mathcal{F}(= \langle u_i f_{e,i} \rangle)$ is the energy production contributed from large-scale forcing and the second term is mean dissipation rate of the kinetic energy. The third term $\varepsilon_p = -\langle u_i f_i \rangle$. However, $\langle u_i f_i \rangle$ is the work done by the polymers to fluid, which is negative in most cases since the spring force of a polymer tends to suppress stretching motion of fluid. Therefore, ε_p is positive. Time-averaged value $\psi_p = \overline{\varepsilon_p}$ along with ε and q is illustrated in Fig. 7(b), clearly indicating that as We increases ψ_p increases while ε decreases. In the previous studies [11,19], in which two-way coupling simulations were performed by using FENE and FENE-P models, the energy decay due to polymers in both decaying and stationary turbulence was computed by using polymer stress tensor. However, in the present study this force is computed by using point-force approximation. Due to the two-way coupling force, the kinetic energy is transferred to the elastic energy of polymers. This term is responsible for the extraction of energy from turbulence in the two-way coupling, as suggested in both particle- and polymer-laden turbulent flow studies [11,19,23,37,38]. The spectral analysis of turbulent kinetic energy is further discussed related to this term in Sec. III B 3.

The statistical comparison of several representative turbulence quantities for both polymer-free and polymer-laden cases is provided for different values of τ_p listed in Table III. The values of the Kolmogorov length and timescales of the modified turbulence, η_k and τ_k, increase as the value of We is increased. This increment is observed due to the reduction in the dissipation ε, as shown in Fig. 7(b). The eddy length l_e and turnover time T_e increase for all values of We, because there exists a reduction in the rms of fluid velocity, which can be seen from the reduction in the mean fluid kinetic energy as shown in Fig. 7(b). The Taylor microscale λ increases for large values of elasticity parameters. The spatial resolution of a spectral simulation [30,39,40] depends on the value of $\kappa_{\max} \eta_k$, which should be greater than 1, for correct simulation of low-order statistics such as mean, rms of velocity, and dissipation. For high-order statistics such as skewness and flatness, the value must be greater than 1.5. The values of $\kappa_{\max} \eta_k$ listed in Table III clearly fulfill the spatial resolution requirement.

As shown in Fig. 7(b), when We = 0.1 and 0.5, the kinetic energy and dissipation are the same as the corresponding values for the unladen turbulence and ψ_p is almost zero, indicating that the polymers remain in the coiled configuration. For We = 1.03 and 2.06, a slight increment in q and ε is observed. Then, both q and ε decrease when We $\geqslant$ 2.97, where the coil-stretch transition in polymers is observed. The polymers start stretching and contribute to the polymers' feedback force. The suppression in dissipation and kinetic energy tend to reach maximum as the elasticity parameter further increases. The contribution of the feedback force f_i increases for large values of We. The role of feedback force in the extraction of energy from turbulence is increased. When We $\geqslant$ 2.06, ψ_p is enhanced.

The PDF of local fluid dissipation is presented for different Weissenberg numbers in Fig. 8. The probability in the low dissipation region is enhanced as the elasticity parameter is increased as shown in the plot in the linear scale in Fig. 8(a). However, when the PDF expressed on the log scale, we find that the probability at the high dissipation region is reduced monotonically with We more significantly as compared to the low dissipation region. This indicates that high dissipation regions are suppressed in the presence of polymers. This reduction is more pronounced for larger Weissenberg numbers as presented in Table III, where the mean dissipation is reduced significantly from We = 0.1 to We = 80 owing to the highly intermittent nature of local dissipation.
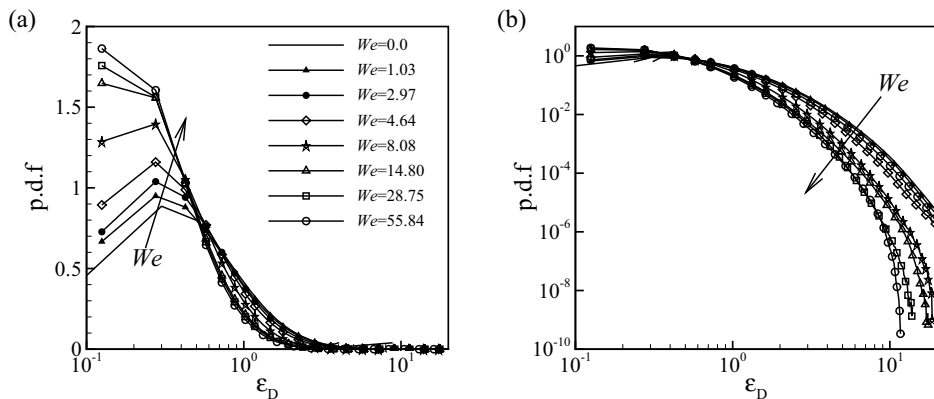
FIG. 8. Effect of polymers on the probability density function of local fluid dissipation for different values of We.

2. Effect of polymers on vorticity

In this section, we investigate the vorticity dynamics as modified by the polymers since the stretching motion of the fluid, which is responsible for the polymer stretching, is mostly caused by coherent rotational structures in turbulence. The vorticity equation derived from Naiver-Stokes equations is

$$\frac{D\omega_i}{Dt} = \omega_j s_{ij} + \nu_f \frac{\partial^2 \omega_i}{\partial x_j \partial x_j} + \epsilon_{ijk} \frac{\partial f_k}{\partial x_j} + \epsilon_{ijk} \frac{\partial f_{e,k}}{\partial x_j}, \tag{13}$$

where the terms on the right-hand side represent the vortex stretching, viscous diffusion, the direct effect of polymers on vorticity, and contribution by the artificial forcing, respectively. First, we focus on the alignment between the vorticity vector and the first two terms on the right-hand side of Eq. (13), the vortex stretching and viscous diffusion of vorticity. For this purpose, the PDF of $\cos\theta_{1,2} = \omega_i W_i/|\omega_i||W_i|$, where $\theta_{1,2}$ is the angle between vorticity vector and W_i, where either $W_i = \omega_j s_{ij}$ or $W_i = \nu_f \partial^2 \omega_i/\partial x_j \partial x_j$. Figure 9 presents the PDF of the cosine angle between vorticity ω_i and vortex stretching W_i for various values of the elasticity parameter compared with the polymer-free case. The maximum probability for the polymer-free case is found to be positively skewed toward 1 as shown in Fig. 9(a), which means that the stretching in vortex dominates over
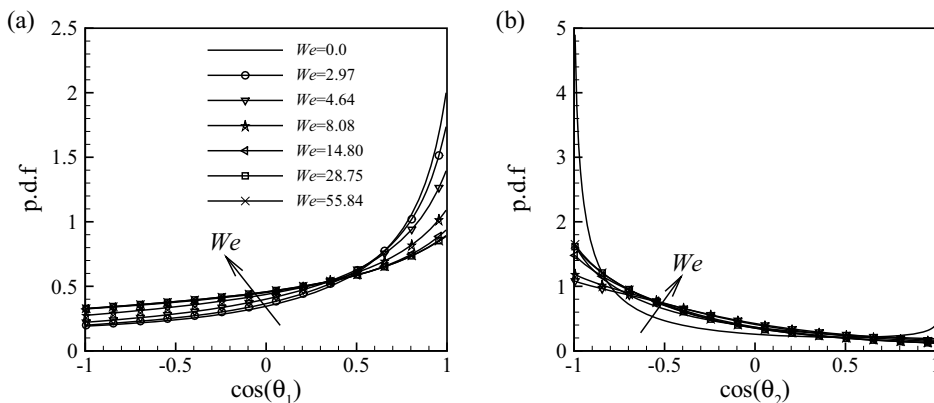

FIG. 9. PDF of the cosine angle between ω_i and (a) $\omega_j s_{ij}$ and (b) $\nu_f \partial^2 \omega_i/\partial x_j \partial x_j$ for various We.

compression, which is consistent with previous studies [4,27]. In the polymer-laden cases, however, the maximum probability near $\theta_1 = 0°$ reduces as We increases compared to the polymer-free case. This indicates that the vortex stretching process is suppressed by polymers in such a way that vorticity and stretching are less parallel with each other than the polymer-free case. Meanwhile, we find that the PDF of the cosine angle increases where $\theta_1 = 180°$, as the elasticity parameter increases. This shows that the probability that ω_i and W_i are antiparallel is higher, which ultimately strengthens the vortex compression.

The PDF of the cosine angle between ω_i and $W_i = \nu_f \partial^2 \omega_i / \partial x_j \partial x_j$ shown in Fig. 9(b) indicates that polymers clearly modify the dynamics of vorticity diffusion. While for the polymer-free case, a large value for the PDF is observed at $\cos \theta_2 = -1$, indicating the strong antialignment, for the polymer case, the peak value of PDF is reduced, implying the suppression of the antialignment by the polymers. However, when $-0.7 < \cos \theta_2 < 0.5$, the PDF of the polymer-laden case is larger than that of the polymer-free case, which indicates that vorticity and viscous diffusion of vorticity tend to be more orthogonal. The vorticity orientation is influenced in the two-way coupling case, when W_i acts perpendicular to vorticity. This behavior is opposite to that of the angle between vorticity vector and vortex stretching vector shown in Fig. 9(a).

The polymer stress tensor defined by $\tau_{ij}^p = \frac{\nu_f \beta}{\tau_p} (\frac{L_{\text{box}}^3}{N_r}) \sum_1^{N_r} [\frac{Q_i^{(m)} Q_j^{(m)}}{Q_0^2} \gamma(z) - \delta_{ij}] \delta(\boldsymbol{x} - \boldsymbol{Q}_c^{(m)})$ has been used to describe the polymer influence on turbulence [4,18,19,27,41]. The gradient of the polymer stress tensor ($\partial \tau_{ij}^p / \partial x_j$) is the feedback force added to the Naiver-Stokes equations. In the previous studies on drag reduction induced by polymers in wall-bounded turbulent flows [37,38,41], it was found that highly stretched polymers remain in the near-wall region and the direct interaction between polymers and the near-wall structures result in the suppression of the quasi-streamwise vortices. The spatial gradients of the polymer stress tensor produced two effects, one opposing the motion of the vortices by gradients [38] and the other extracting energy from the vortices and transferring it to the polymers [42]. The feedback force in the current study is based on the elastic force between the two beads. The feedback force from polymers on turbulence depends on the spring constant H, which is inversely proportional to the polymer relaxation time τ_p, or We. The large We indicates that the polymers stretch over a longer period. The polymers are influenced by the stretching due to the fluid motion. We find that the highly stretched polymers are preferentially found around the vortical structures as shown in Fig. 11(a), and these structures are suppressed by the polymer feedback force. This finding is similar to what previous studies reported for wall-bounded turbulent flows [37,38,41].

Figure 10 presents the comparison of isosurface of the vorticity magnitude $|\omega_i|$ for one-way coupling and two-way coupling cases at We = 2.97, 4.64 and 8.08. Previous studies [43,44] without polymers related to DNS of homogeneous isotropic turbulence suggested that for large value of $|\omega_i|$, isosurfaces are filamentary. Recently Perlekar *et al.* [10] performed the DNS of stationary turbulence in the presence of polymer additives in which they used the FENE-P model. They found that in the presence of polymers the filaments are suppressed and this suppression is more pronounced as We increases. In the current study using the FENE model, we observe similar behavior and found that for large values of We the suppression is more pronounced, as shown in Figs. 10(b), 10(c), and 10(d).

The PDF of the cosine angle $\cos \theta_3 = \boldsymbol{Q} \cdot \boldsymbol{\omega} / |\boldsymbol{Q}||\boldsymbol{\omega}|$ is computed to investigate the alignment between these two vectors. The PDF is shown for We = 4.64 and We = 55.84 for both one-way and two-way coupling cases in Fig. 11(b). In the one-way coupling case, the peak value of probability is observed at approximately 1 for all chosen Weissenberg numbers, which means that $\boldsymbol{Q}$ and $\boldsymbol{\omega}$ tend to be parallel to each other. However, in the case of two-way coupling for We = 4.64, the peak value at 1 decreases compared to one-way case. This explains why vortex compression is observed more often than vortex stretching in the presence of polymers. The back-reaction force from polymers plays a role in the suppression of the vortex tube. The reduction in the peak value at 1 is more pronounced in the case of We = 14.80. This reduction is more significant in the case of We = 55.84 as shown in the inset of Fig. 11(b).
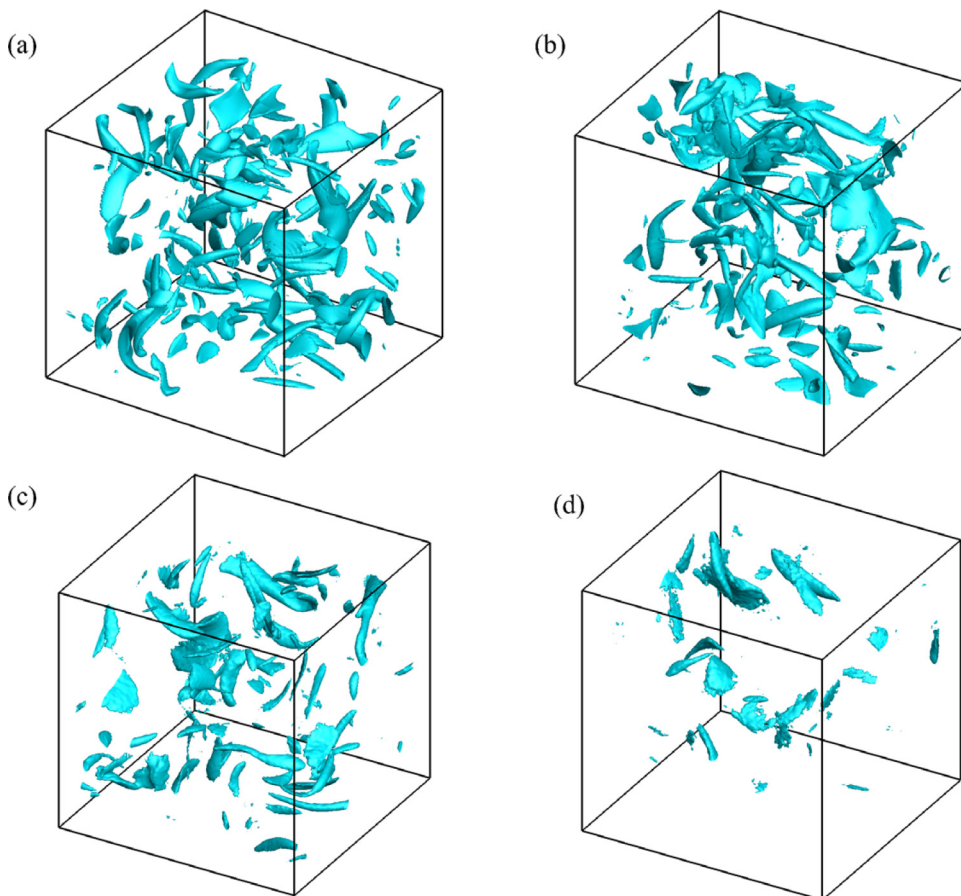
FIG. 10. Comparison of the isosurfaces of $|\omega_i|$ in flow (a) without polymers and [(b), (c), (d)] with polymers at We = 2.97, 4.64, 8.08,. The level is chosen by $|\omega_i|/\sigma_\omega = 3.5$. where σ_ω is the standard deviation of $|\omega_i|$.
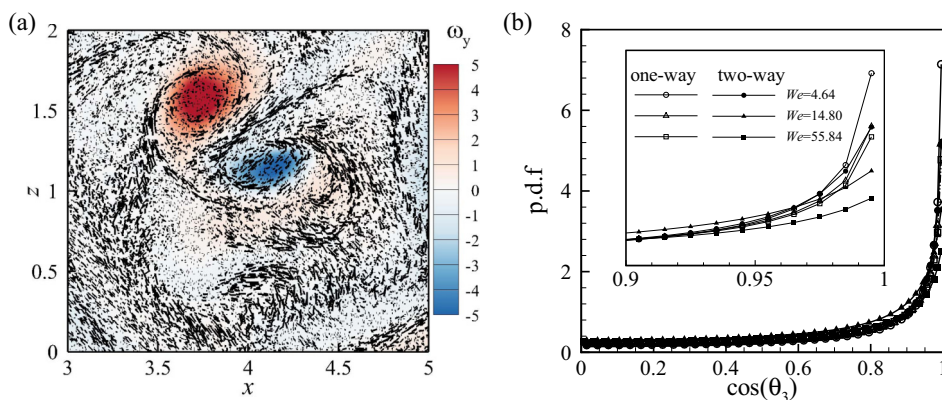

FIG. 11. (a) Distribution of end-to-end distance vector along with fluid vorticity component in an x-z plane for We = 2.97 and (b) PDF of the cosine angle between the end-to-end distance and vorticity vector, open symbol corresponds to the one-way case, while closed represents two-way coupling case. Inset shows an enlarged view for $0.9 \leqslant \cos\theta_3 \leqslant 1.0$.
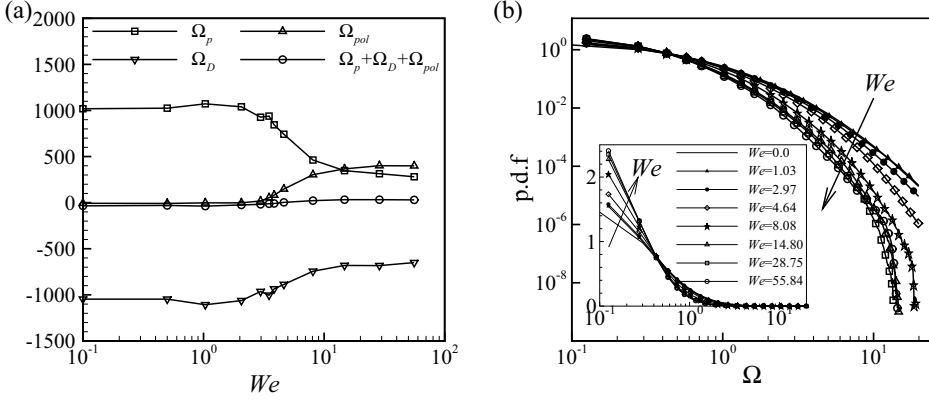
FIG. 12. Influence of the Weissenberg number on (a) average enstrophy production, dissipation, the polymer contribution, and the sum of all three and (b) PDF of Ω with inset in linear vertical scale.

For a better interpretation of the effect of polymers on vorticity, we further investigate the dynamics of vorticity through the dynamics equation of enstrophy given by

$$\frac{D}{Dt}\left(\frac{1}{2}\langle \omega_i \omega_i \rangle\right) = \langle \omega_i \omega_j s_{ij} \rangle + \nu_f \left\langle \omega_i \frac{\partial^2 \omega_i}{\partial x_j \partial x_j} \right\rangle + \epsilon_{ijk}\left\langle \omega_i \frac{\partial f_k}{\partial x_j} \right\rangle + \epsilon_{ijk}\left\langle \omega_i \frac{\partial f_{e,k}}{\partial x_j} \right\rangle, \qquad (14)$$

where terms on the right-hand side represent the averaged enstrophy production, dissipation, polymer effect on enstrophy transport, and the contribution by the artificial force, respectively. The time-averaged quantities are represented as $\Omega = \frac{1}{2}\overline{\langle \omega_i \omega_i \rangle}$, $\Omega_p = \overline{\langle \omega_i \omega_j s_{ij} \rangle}$, $\Omega_D = \nu_f \overline{\langle \omega_i \nabla^2 \omega_i \rangle}$, and $\Omega_{\text{pol}} = \epsilon_{ijk}\overline{\langle \omega_i \frac{\partial f_k}{\partial x_j} \rangle}$. The contribution by the artificial force is not investigated since it is negligibly small. The computed values of average enstrophy production, dissipation, polymer contribution, and the sum of all three terms are presented in Fig. 12(a). The polymer contribution is negligible for We $\leqslant 2.06$, and thus production is balanced by dissipation. The monotonic decay in the average enstrophy production is observed when We $\geqslant 2.97$. The decay in time-averaged value is due to feedback forces, as we observed that the vorticity generation is suppressed in the polymer-laden flow. It is noteworthy that the direct contribution to enstrophy of the feedback forces is positive but they also suppress vortex stretching, resulting in significant suppression of enstrophy production. Enstrophy dissipation is also suppressed by the polymer feedback forces.

The PDF distribution of local enstrophy Ω is shown in Fig. 12(b). The effect of polymers on the distribution of Ω becomes significant as the Weissenberg number increases. PDF for the low enstrophy region increases, while PDF for the high enstrophy region decreases as the elasticity parameter increases. The reduction at the high enstrophy region is more prominent than the low enstrophy region, resulting in an overall reduction in $\langle \Omega \rangle$ as the Weissenberg number increases. These results are in qualitative agreement with the experimental study [45] wherein dilute polymer solution was investigated.

3. Spectral analysis

Finally, we investigated the spectral dynamics of the two-way coupling between polymers and turbulence. Although the scale of the stretched polymers is extremely small, the effect of the feedback forces extends to various large-scale motions of the fluid through the energy exchange between different scales. To observe the effect of We* on spectral dynamics, the kinetic energy equation in spectral space was investigated [20],

$$\frac{dE(\kappa)}{dt} = T_e(\kappa) - \varepsilon(\kappa) - \psi_p(\kappa) + \mathcal{F}(\kappa), \qquad (15)$$
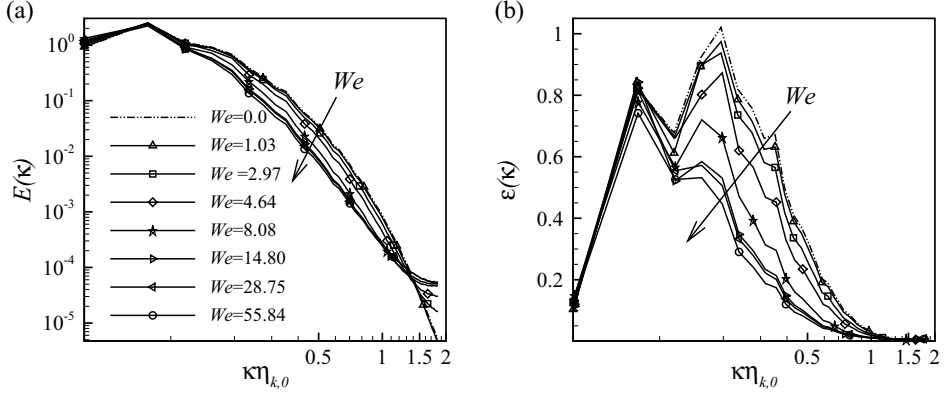
FIG. 13. (a) Three dimensional kinetic energy (b) dissipation spectra for different values of We.

where $\kappa = |\boldsymbol{\kappa}|$ is the magnitude of the wave-number vector. $E(\kappa)$ represents the energy spectrum, $T_e(\kappa)$ is the spectral energy transfer rate, $\varepsilon(\kappa)$ is the dissipation rate spectrum, and $\psi_p(\kappa)$ is the rate of the two-way interaction energy. $\mathcal{F}$ denotes the contribution of the artificial force to maintain turbulence. These terms are expressed respectively as [20]

$$E(\kappa) = \sum_{\kappa \leqslant |\boldsymbol{\kappa}| < \kappa+1} \frac{1}{2}\big[\hat{u}_j^*(\boldsymbol{\kappa})\hat{u}_j(\boldsymbol{\kappa})\big], \qquad T_e(\kappa) = \sum_{\kappa \leqslant |\boldsymbol{\kappa}| < \kappa+1} \text{Re}\big\{\hat{u}_j^*(\boldsymbol{\kappa})\widehat{NL}_j(\boldsymbol{\kappa})\big\}, \tag{16}$$

$$\varepsilon(\kappa) = 2\nu\kappa^2 \sum_{\kappa \leqslant |\boldsymbol{\kappa}| < \kappa+1} \frac{1}{2}\big[\hat{u}_j^*(\boldsymbol{\kappa})\hat{u}_j(\boldsymbol{\kappa})\big], \qquad \psi_p(\kappa) = -\sum_{\kappa \leqslant |\boldsymbol{\kappa}| < \kappa+1} \text{Re}\big\{\hat{u}_j^*(\boldsymbol{\kappa})\hat{f}_j(\boldsymbol{\kappa})\big\}, \tag{17}$$

where $\hat{u}_j$ and $\hat{u}_j^*$ denote the Fourier coefficient of u_j and its complex conjugate, respectively. $\widehat{NL}_i(\boldsymbol{\kappa}) = \hat{H}_i - \kappa_i\kappa_j\hat{H}_j/\kappa^2$ is the Fourier coefficient of the projected nonlinear term of the Navier-Stokes equation and $\hat{H}_i = \varepsilon_{ijk}\hat{u}_j\hat{\omega}_k$ with $\hat{\omega}_k$ denoting the Fourier coefficient of vorticity vector. Re indicates the real part of a complex variable. $\hat{f}_j$ is the Fourier coefficient of the feedback force from polymers.

In Figs. 13 and 14, we show the turbulence spectra and the spectral two-way coupling energy rate for various Weissenberg numbers. As shown in Fig. 13(a), when We $\leqslant$ We$_{\text{CST}}$($= 2.97$), the
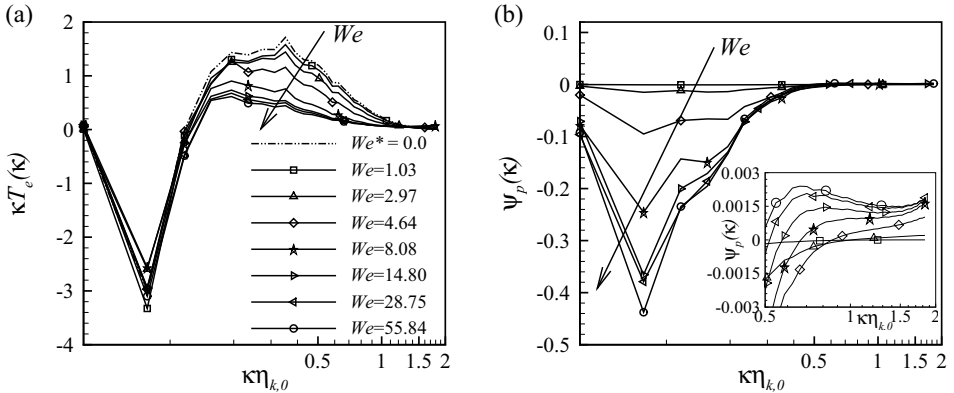

FIG. 14. Polymers influence on (a) energy transfer function (b) and two-way interaction energy rate due to polymers.

kinetic energy spectrum is hardly modified by the two-way coupling feedback. When We > 2.97, however, energy in the range $0.2 \leqslant \kappa\eta_{k,0} \leqslant 1.5$, is suppressed, whereas small-scale components in the range $1.5 < \kappa\eta_{k,0}$ are enhanced. In their DNS study of stationary isotropic turbulence at $Re_\lambda = 80$, Perlekar *et al.* [10] also showed, using the FENE-P model, that the kinetic energy spectrum decreases at intermediate wave numbers for similar Weissenberg numbers (Weissenberg numbers of 3.5 and 7.1 based on the Kolmogorov timescale of the polymer-free flow). They further conducted a high-resolution, low-Re_λ DNS without aliasing errors to demonstrate that polymer additives enhance the kinetic energy spectrum in the deep dissipation range. In Fig. 13(a), the modification due to polymers seems to be saturated as We is further increased. Owing to the suppression in most scales, the total kinetic energy decreases as listed in Table III.

The dissipation spectra presented in Fig. 13(b) show similar behavior to the kinetic energy spectra. The dissipation spectrum for polymer-free case shows two peaks, the one of which at $\kappa\eta_{k,0} = 0.088$ is due to the external forcing to maintain turbulence, similar to the peak in the energy spectrum shown in Fig. 13(a). For We $\leqslant$ 2.97, the modification is negligible. When We > 2.97, the dissipation is suppressed in most of the ranges of scales. Particularly, the suppression in the range $0.2 \leqslant \kappa\eta_{k,0} \leqslant 1.0$ is significant although the suppression becomes saturated as We is further increased. A slight increase in the dissipation spectra on a small scale is negligible, resulting in more suppression in the total dissipation than the total kinetic energy, as shown in Table III.

The effect of polymers on the energy transfer between different scales is displayed in Fig. 14(a). The negative peak on a large scale is hardly modified by polymers, whereas for $0.175 < \kappa\eta_{k,0} \leqslant 1.0$, the monotonic suppression of the positive energy transfer is observed as We increases. Figure 14(b) presents the direct contribution of polymers to the spectral energy. For all Weissenberg numbers, the spectral two-way coupling energy rate is negative at low wave numbers, with a peak at $\kappa\eta_{k,0} \approx 0.1$, where large-scale energy is supplied from the forcing. This indicates that despite their small size (smaller than the Kolmogorov scale), stretched polymers collectively interact with large-scale turbulent motions, as clearly seen in Fig. 11(a) and as explained by Watanabe and Gotoh [18]. The negative contribution of $\psi_p(\kappa)$ at low wave numbers is also consistent with previous observations from Eulerian-Eulerian simulations of steady isotropic turbulence and homogeneous shear turbulence with the FENE-P model ([11,12]; [46]) and from Eulerian-Lagrangian simulations of decaying isotropic turbulence with the dumbbell model (Watanabe and Gotoh [18]). It is worth noting that Watanabe and Gotoh [18] showed that in decaying isotropic turbulence, a positive contribution of $\psi_p(\kappa)$ at $\kappa\eta_k > 1$ is responsible for the formation of a power-law decay of the kinetic energy spectrum, for their largest Weissenberg number (Weissenberg number of 25 based on the Kolmogorov timescale of the polymer-free case when the dissipation rate reaches its maximum value). Valente *et al.* [12] also found a transfer of energy from elastic to kinetic energies at high wave numbers when the polymer relaxation time is large (Weissenberg numbers of We $\approx$ 5 and 10) in their DNS of steady isotropic turbulence with the FENE-P model. Consistent with these observations, positive $\psi_p(\kappa)$ is also observed at high wave numbers in our Eulerian-Lagrangian simulation of steady isotropic turbulence with the dumbbell model, as shown in the inset of Fig. 14(b), although the magnitude of ψ_p is quite small compared to the negative contribution at large scales. In the inset of Fig. 14(b), as the Weissenberg number increases, the positive contribution of $\psi_p(\kappa)$ becomes significant progressively toward low wave numbers. For our two largest We, positive peaks appear at $\kappa\eta_k \approx 0.6$. The effect of We on the turbulence spectra and the two-way coupling energy rate spectrum is consistent with the We dependence of polymer stretch shown in Fig. 3(a).

IV. CONCLUSION

In this paper, the direct numerical simulation of polymer-laden homogeneous isotropic turbulence was performed using the Eulerian-Lagrangian approach to investigate the two-way coupling effect. The polymer tracking was carried out by adopting the finitely extensible nonlinear elastic dumbbell model. The parametric study of the Weissenberg number was performed to investigate the polymers' stretching and its effect on turbulence modification. The spring force between

two beads was modeled as a back-reaction force from polymers on turbulence through the point force approximation. We found that at the volume fraction $\phi_v = 2.525 \times 10^{-6}$, the N number of polymers, where $N_c = O(10^7)$, is sufficient to observe the converged turbulence modification. Therefore, direct implementation of a pair of feedback forces is more efficient than the polymer stress approach.

The polymer statistics were computed for the end-to-end distance vector magnitude. When We $\leqslant 2.06$, the polymers are not significantly stretched and thus most polymers remain in a coiled configuration. We note that the stretching of polymers is limited owing to the presence of a two-way coupling force, compared to one-way coupling. The stretching phenomenon in polymers is characterized by the PDF of the end-to-end distance vector magnitude. For large Weissenberg numbers, the polymers are stretched closer to the maximum value. The coil-stretch transition is investigated for the two-way coupling simulation. The coil-stretch transition in polymers occurs when We $= 2.97$ or We* $= 3.0$. This finding is similar to the one-way coupling result, where the coil-stretch transition for passive polymers in stationary turbulence was reported when We $= 3.0$–4.0.

The alignment between the end-to-end distance vector, vorticity vector, and eigenvectors of strain-rate tensor was investigated. In the case of the end-to-end distance vector, we found that when We* < 10, the polymers are preferentially aligned along the σ_1 direction, the most stretching direction of rate of strain tensor. However, for We* $= 20, 80$, the polymers tend to align along the σ_2 direction corresponding to the intermediate eigenvalue, and the probability that the polymers aligned along the σ_1 direction is reduced. An investigation of the alignment between the vorticity vector and the eigenvectors of rate of strain tensor revealed that when We* $= 5.0$, the vorticity vector has a tendency to preferentially align along either the σ_1 or σ_2 direction. However, the alignment trend when We* $= 20, 80$ is similar to that of the end-to-end distance vector. With an increase in the Weissenberg number, the probability that the vorticity vector and the eigenvector of rate of strain tensor are parallel decreases.

No substantial modification in turbulence was observed when We $\leqslant 2.06$. When We $\geqslant 2.97$, however, polymers are substantially stretched, and they contributed more to turbulence modification. The turbulent kinetic energy on large scales and dissipation on small scales were reduced as We increased. The polymers extract the kinetic energy from the fluid and store in the form of elastic energy. The polymers store maximum elastic energy when We $= 8.08$, and for higher We the elastic energy is stored less due to attenuation in turbulence.

The polymers rotate around the vortical structures, and highly stretched polymers are observed at the edge of vortical structures. The vortical structures are more suppressed as the elasticity parameter increased. Polymers contribute to maintaining the turbulence, when the enstrophy production is reduced for large We. The antialignment trend between the vorticity and the vortex stretching vector increases when the elasticity parameter increases, thus indicating that the role of the polymers is vortex compression instead of vortex stretching. The augmentations in kinetic energy spectra were observed on both large and small scales for all values of We. The two-way interaction energy rate is dependent on the choice of the Weissenberg number. The decay in dissipation spectra is found at the intermediate wave numbers.

We present a detailed study on polymers and their interaction with isotropic turbulence for a wide range of Weissenberg numbers. Although polymers have been known to be responsible for the suppression of turbulence for a long time, our approach based on direct forcing in stationary turbulence showed a potential for a more physical insight. Similar investigation on anisotropic turbulence such as shear flow or near-wall turbulence would be interesting. Particularly, the drag reduction mechanism in polymer-laden boundary layer flow could be investigated under the Lagrangian treatment of polymer dynamics.

[1] B. A. Toms, Some observations on the flow of linear polymer solutions through straight tubes at large Reynolds numbers, in *Proceedings of the 1st International Congress of Rheology* (N. Holland, Amsterdam, 1948), pp. 135–141.

[2] E. D. Burger, W. R. Munk, and H. A. Wahl, Flow increase in the Trans-Alaska Pipeline through use of a polymeric drag-reducing additive, J. Pet. Technol. **34**, 377 (1982).

[3] R. B. Bird, *Dynamics of Polymeric Liquids* (Wiley, New York, 1977).

[4] W.-H. Cai, F.-C. Li, and H.-N. Zhang, Direct numerical simulation study of the interaction between the polymer effect and velocity gradient tensor in decaying homogeneous isotropic turbulence, Chin. Phys. B **20**, 124702 (2011).

[5] E. De Angelis, C. Casciola, R. Benzi, and R. Piva, Homogeneous isotropic turbulence in dilute polymers, J. Fluid Mech. **531**, 1 (2005).

[6] C. D. Dimitropoulos, Y. Dubief, E. S. Shaqfeh, P. Moin, and S. K. Lele, Direct numerical simulation of polymer-induced drag reduction in turbulent boundary layer flow, Phys. Fluids **17**, 011705 (2005).

[7] C. D. Dimitropoulos, R. Sureshkumar, and A. N. Beris, Direct numerical simulation of viscoelastic turbulent channel flow exhibiting drag reduction: Effect of the variation of rheological parameters, J. Non-Newtonian Fluid Mech. **79**, 433 (1998).

[8] R. Sureshkumar, A. N. Beris, and R. A. Handler, Direct numerical simulation of the turbulent channel flow of a polymer solution, Phys. Fluids **9**, 743 (1997).

[9] P. Ilg, E. De Angelis, I. Karlin, C. Casciola, and S. Succi, Polymer dynamics in wall turbulent flow, EPL **58**, 616 (2002).

[10] P. Perlekar, D. Mitra, and R. Pandit, Direct numerical simulations of statistically steady, homogeneous, isotropic fluid turbulence with polymer additives, Phys. Rev. E **82**, 066313 (2010).

[11] P. C. Valente, C. B. da Silva, and F. T. Pinho, The effect of viscoelasticity on the turbulent kinetic energy cascade, J. Fluid Mech. **760**, 39 (2014).

[12] P. C. Valente, C. B. da Silva, and F. T. Pinho, Energy spectra in elasto-inertial turbulence, Phys. Fluids **28**, 075108 (2016).

[13] S. Jin and L. R. Collins, Dynamics of dissolved polymer chains in isotropic turbulence, New J. Phys. **9**, 360 (2007).

[14] T. Watanabe and T. Gotoh, Coil-stretch transition in an ensemble of polymers in isotropic turbulence, Phys. Rev. E **81**, 066301 (2010).

[15] D. Vincenzi, P. Perlekar, L. Biferale, and F. Toschi, Impact of the Peterlin approximation on polymer dynamics in turbulent flows, Phys. Rev. E **92**, 053004 (2015).

[16] T. Peters and J. Schumacher, Two-way coupling of finitely extensible nonlinear elastic dumbbells with a turbulent shear flow, Phys. Fluids **19**, 065109 (2007).

[17] T. Watanabe and T. Gotoh, Kinetic energy spectrum of low-Reynolds-number turbulence with polymer additives, J. Phys.: Conf. Ser. **454**, 012007 (2013).

[18] T. Watanabe and T. Gotoh, Hybrid Eulerian-Lagrangian simulations for polymer-turbulence interactions, J. Fluid Mech. **717**, 535 (2013).

[19] T. Watanabe and T. Gotoh, Power-law spectra formed by stretching polymers in decaying isotropic turbulence, Phys. Fluids **26**, 035110 (2014).

[20] A. Ferrante and S. Elghobashi, On the physical mechanisms of two-way coupling in particle-laden isotropic turbulence, Phys. Fluids **15**, 315 (2003).

[21] A. H. Abdelsamie and C. Lee, Decaying versus stationary turbulence in particle-laden isotropic turbulence: Turbulence modulation mechanism, Phys. Fluids **24**, 015106 (2012).

[22] A. H. Abdelsamie and C. Lee, Decaying versus stationary turbulence in particle-laden isotropic turbulence: Heavy particle statistics modifications, Phys. Fluids **25**, 033303 (2013).

[23] J. Lee and C. Lee, Modification of particle-laden near-wall turbulence: Effect of Stokes number, Phys. Fluids **27**, 023303 (2015).

[24] B. Gereltbyamba and C. Lee, Flow modification by inertial particles in a differentially heated cubic cavity, Int. J. Heat Fluid Flow **79**, 108445 (2019).

[25] J. Lee and C. Lee, The effect of wall-normal gravity on particle-laden near-wall turbulence, J. Fluid Mech. **873**, 475 (2019).

[26] H. Shim and C. Lee, Two-way interaction between isotropic turbulence and dispersed bubbles, J. Mech. Sci. Technol. **35**, 1527 (2021).

[27] W.-H. Cai, F.-C. Li, and H.-N. Zhang, DNS study of decaying homogeneous isotropic turbulence with polymer additives, J. Fluid Mech. **665**, 334 (2010).

[28] B. Eckhardt, J. Kronjäger, and J. Schumacher, Stretching of polymers in a turbulent environment, Comput. Phys. Comm. **147**, 538 (2002).

[29] M. Fujimura, T. Atsumi, H. Mamori, K. Iwamoto, A. Murata, M. Masuda, and H. Ando, Numerical simulation of drag-reducing channel flow by using bead-spring chain model, Int. J. Heat Fluid Flow **63**, 75 (2017).

[30] V. Eswaran and S. Pope, An examination of forcing in direct numerical simulations of turbulence, Comput. Fluids **16**, 257 (1988).

[31] J.-I. Choi, K. Yeo, and C. Lee, Lagrangian statistics in turbulent channel flow, Phys. Fluids **16**, 779 (2004).

[32] N. T. Ouellette, H. Xu, and E. Bodenschatz, Bulk turbulence in dilute polymer solutions, J. Fluid Mech. **629**, 375 (2009).

[33] S. Elghobashi and G. Truesdell, On the two-way interaction between homogeneous turbulence and dispersed solid particles. I: Turbulence modification, Phys. Fluids **5**, 1790 (1993).

[34] P. De Gennes, Coil-stretch transition of dilute flexible polymers under ultrahigh velocity gradients, J. Chem. Phys. **60**, 5030 (1974).

[35] K. R. Sreenivasan and C. M. White, The onset of drag reduction by dilute polymer additives, and the maximum drag reduction asymptote, J. Fluid Mech. **409**, 149 (2000).

[36] P. E. Hamlington, J. Schumacher, and W. J. Dahm, Direct assessment of vorticity alignment with local and nonlocal strain rates in turbulent flows, Phys. Fluids **20**, 111703 (2008).

[37] C. M. White and M. G. Mungal, Mechanics and prediction of turbulent drag reduction with polymer additives, Annu. Rev. Fluid Mech. **40**, 235 (2008).

[38] Y. Dubief, V. E. Terrapon, C. M. White, E. S. Shaqfeh, P. Moin, and S. K. Lele, New answers on the interaction between polymers and vortices in turbulent flows, Flow, Turbul. Combust. **74**, 311 (2005).

[39] S. B. Pope, *Turbulent Flows* (IOP, London, 2001).

[40] P.-K. Yeung and S. B. Pope, Lagrangian statistics from direct numerical simulations of isotropic turbulence, J. Fluid Mech. **207**, 531 (1989).

[41] V. Terrapon, Y. Dubief, P. Moin, E. S. Shaqfeh, and S. K. Lele, Simulated polymer stretch in a turbulent flow using Brownian dynamics, J. Fluid Mech. **504**, 61 (1999).

[42] P. Ptasinski, B. Boersma, F. Nieuwstadt, M. Hulsen, B. Van den Brule, and J. Hunt, Turbulent channel flow near maximum drag reduction: Simulations, experiments, and mechanisms, J. Fluid Mech. **490**, 251 (2003).

[43] Y. Kaneda, T. Ishihara, M. Yokokawa, K. Itakura, and A. Uno, Energy dissipation rate and energy spectrum in high resolution direct numerical simulations of turbulence in a periodic box, Phys. Fluids **15**, L21 (2003).

[44] R. Pandit, P. Perlekar, and S. S. Ray, Statistical properties of turbulence: An overview, Pramana **73**, 157 (2009).

[45] A. Liberzon, M. Guala, W. Kinzelbach, and A. Tsinober, On turbulent kinetic energy production and dissipation in dilute polymer solutions, Phys. Fluids **18**, 125101 (2006).

[46] A. Robert, T. Vaithianathan, L. R. Collins, and J. G. Brasseur, Polymer-laden homogeneous shear-driven turbulent flow a model for polymer drag reduction, J. Fluid Mech. **657**, 189 (2010).